CHEMICAL ENGINEERING TRANSACTIONS
VOL. 117, 2025
A publication of AIDIC
The Italian Association of Chemical Engineering
Online at www.cetjournal.it
Guest Editors: Fabrizio Bezzo, Flavio Manenti, Gabriele Pannocchia, Almerinda di Benedetto

ISBN 979-12-81206-17-5; **ISSN** 2283-9216
DOI: 10.3303/CET25117124

Hydrogen Production from Wastewater: using the Photo-Electrochemical (PEC) Approach to Recover High-Value Products

Francesco Tavella*, Daniele Giusi, Luana De Pasquale, Victor Longo, Davide Cosio, Lavanya Veerapuram, Chiara Genovese, Claudio Ampelli

Department of Chemical, Biological, Pharmaceutical and Environmental Sciences (ChiBioFarAm) – University of Messina, ERIC aisbl and CASPE/INSTM, Viale Ferdinando Stagno d'Alcontres, 31 - 98166 Sant'Agata di MESSINA (Italy)
ftavella@unime.it

The present work focuses on developing a versatile photo-electrochemical (PEC) system designed to operate in both gas and liquid phases for the photo-upgrading of ethanol. This device, made of Plexiglas, was developed adopting a modular approach. It consists of two gas-tight half-cells separated by a reinforced proton-exchange membrane and connected to two small tanks for electrolytes, which also serve as gas storage. The photo-electrode used is a membrane of TiO_2 nanotubes supported onto a Ti mesh. This novel 2D-3D electrode, located in direct contact with the exchange membrane, enables gas-phase (zero-gap) operation and shows superior performance in terms of photocurrent generation and reduced ohmic resistance. The photo-reforming tests were conducted using a 20% ethanol solution in water as the anolyte and a 0.050 M Na_2SO_4 aqueous solution as the catholyte. Hydrogen (H_2) production rates of 11.2 μmol h^{-1} and 6.5 μmol h^{-1} were obtained in the gas-phase (GP) and liquid-phase (LP) configurations, respectively. Note that in the GP configuration, an inert gas stream transported the ethanol vapour to the anode operating in gas phase. Interestingly, the LP configuration yielded higher production rates of value-added chemicals, including 13.3 μmol h^{-1} of acetaldehyde and 0.4 μmol h^{-1} of acetic acid, compared to the GP configuration, which produced 4.2 μmol h^{-1} of acetaldehyde and no detectable acetic acid. These results demonstrate that photo-electrocatalytic performance is governed not only by the catalyst but also by the device configuration and type of operation.

1. Introduction

Photo-electrochemical (PEC) cells offer a promising technology for sustainable hydrogen (H_2) production. By harnessing solar energy, these devices can efficiently convert water into hydrogen gas, a clean and versatile fuel. Moreover, PEC cells can store intermittent renewable energy sources like solar, wind, and hydropower, ensuring a consistent energy supply (Nabgan et al., 2024). However, most studies focus primarily on the production of H_2 in the cathode compartment of PEC cells (Lima Perini et al., 2021). In contrast, the anode compartment, where oxidation reactions occur, typically produces only oxygen (O_2) if the electrolyte contains only water. However, replacing pure water with solutions containing small organic molecules or dyes, such as wastewater from municipal treatment plants (Hu et al., 2024), bio-refineries (Hu et al., 2017), or textile industries (Verma et al., 2022)., presents a valid alternative. Oxidizing organic pollutants in the anode offers several advantages: a) reducing the cell's overpotential (Ampelli et al., 2023), b) increasing the H_2 production rate, and c) generating highly valuable products (Wei et al., 2024; Yadav et al., 2022). PEC cells are an emerging technology, and various design approaches have been proposed in the literature, from simple H-type cells, suitable for electrode characterization, to more advanced configurations such as membrane electrode assembly (MEA) cells or flow-cells, which are more suitable for the industrial-scale applications (Ampelli et al., 2023).
In this work, a novel modular and versatile PEC cell was developed. The key advantage of this design is its ability to operate in both gas and liquid phases without the need to open the cell or remove the catalytic MEA. Switching between operating conditions (e.g., moving from liquid- to gas-phase configuration) can influence the

Paper Received: 10 January 2025; Revised: 14 March 2025; Accepted: 7 May 2025
Please cite this article as: Tavella F., Giusi D., De Pasquale L., Longo V., Cosio D., Veerapuram L., Genovese C., Ampelli C., 2025, Hydrogen Production from Wastewater: Using the Photo-electrochemical (pec) Approach to Recover High-value Products, Chemical Engineering Transactions, 117, 739-744 DOI:10.3303/CET25117124

selectivity of the process, enabling the catalyst to conduct one or more oxidation/reduction steps (Giusi et al., 2023).Titanium dioxide (TiO_2) nanotubes supported on Ti mesh were selected as the photoactive material due to their unique ability to absorb UV light and suitable bandgap for water-splitting reaction (~3.2 eV). This 2D-3D architectured tubular morphology enhances visible light absorption through scattering phenomena and strongly reduces the charge recombination rate (Saboo et al., 2018) which is one of the main drawbacks of bulk TiO_2 (Ampelli et al 2017). To better understand the performance and limitations of the two cell configurations, electrochemical impedance spectroscopy (EIS) measurements were conducted, thus revealing key bottlenecks and providing insights into the two systems (De Pasquale et al 2023).

2. Experimental

2.1 Electrode preparation

Titanium dioxide nanotubes (TiO_2NTs) were synthesized using a metallic titanium mesh (80 mesh, woven from 0.13 mm diameter wire, Alfa Aesar) as the substrate. The Ti mesh was first sonicated in isopropyl alcohol for 30 minutes to remove any native oxide layer or organic impurities. After drying, the sample was anodized at room temperature through the controlled anodic oxidation technique. The clean substrate was placed in a two-electrode electrochemical cell, made in Teflon, as the working electrode, with a platinum (Pt) electrode serving as the counter electrode. A potentiostat (Agilent E3612A) and a multimeter (Keithley 2000) were used to apply a constant potential of 50 V and monitor the resulting current, respectively. The anodization was conducted for 1 hour under continuous stirring in an electrolyte bath consisting of ethylene glycol with 2.0 wt% deionized water and 0.3 wt% ammonium fluoride. After the anodization, the sample was dried at ambient conditions and later annealed at 450°C for 3 hours, to induce crystallization of the amorphous oxide nanotube arrays into the TiO_2 anatase phase.

2.2 Membrane electrode assembly

The assembly of the electrode materials was critical to ensure proper adherence between layers, to facilitate efficient mass transport and minimize electrical losses. The assembly procedure was the same for both gas-phase and liquid-phase configurations. The photoanode and a Nafion® N324 membrane were cut into circular shapes with a diameter of 36 mm and subsequently brought into contact, with the "anodic" part of the membrane facing the photoanode. To apply additional pressure, a silicon disk of the same diameter was included in the assembly. The assembly was subjected to hot pressing at 130°C for 90 seconds. Then, the silicon disk was easily removed, and the resulting electrode (consisting of the photoanode adhered to the membrane) was placed into the PEC cell for testing.

2.3 Electrochemical device

The PEC cell used for the photo-electrochemical characterization and catalytic tests was designed to operate in both gas-phase (GP) or liquid-phase (LP) configurations. The device was made of Plexiglas, with two separate anodic and cathodic compartments, a quartz window, and multiple inlets and outlets for gases and/or liquids to accommodate the desired operational mode (LP or GP) in two or three-electrode configuration (see Figures 1a and b). For this work, all tests and photo-electrochemical characterizations were performed in a two-electrode configuration, using a square Pt foil with an area of 1 cm^2 as the counter-electrode, and the TiO_2NTs/Ti mesh–based photoanode as the working electrode.

A schematic depiction of the GP setup is shown in Figure 1a. A hot plate maintained a solution of ethanol (20 vol% in deionized water) at a constant temperature of 60°C. A nitrogen flowrate of 20 mL min^{-1} was used to transfer the ethanol vapour from the headspace of the flask to the anodic compartment of the PEC cell. Illumination was provided by a solar simulator (300 W Xe-arc lamp, Quantum Design) placed 5 cm from the cell's quartz window. The cathodic compartment was supplied with an aqueous electrolyte solution (0.050 M H_2SO_4) circulated by a peristaltic pump from an external reservoir containing 40 mL of electrolyte. Hydrogen produced in the cathodic chamber was carried by a nitrogen flow (20 mL min^{-1}) to a micro gas chromatograph (Pollution micro-GC) for analysis. Vapours from the anodic compartment were collected in an absorber containing 1 mL of 0.005 M H_2SO_4 aqueous solution, placed in an ice bath, and then the collected products were analysed using gas chromatography-mass spectrometry (GC-MS, Thermo-Fisher Trace 1310) and ionic chromatography (IC, Metrohm 940 Vario).

In the LP setup (Figure 1b), the ethanol solution (20 vol% in deionized water) was directly sent to the anodic chamber using a peristaltic pump. The same pump (two channels) was also used to recirculate the cathodic electrolyte (0.050 M H_2SO_4). The gaseous products from the cathodic chamber were analysed using the micro-GC, whilst the liquid products from the anodic chambers were sampled every 30 minutes and analysed using GC-MS and IC.

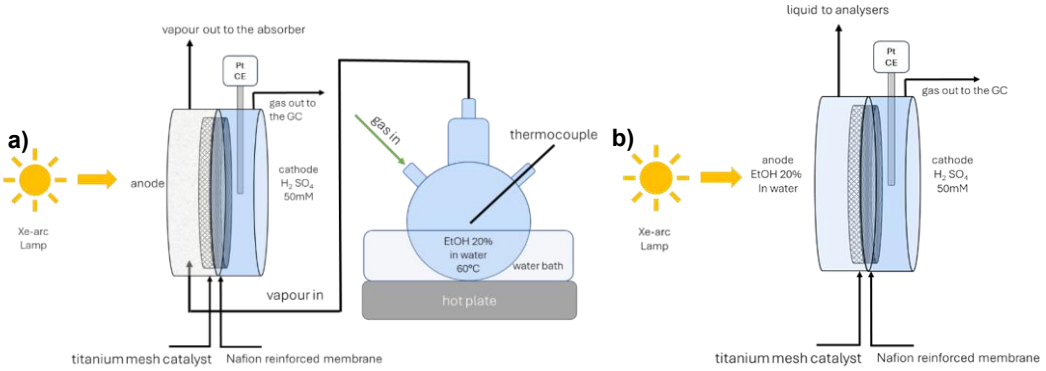

Figure 1: Representative schemes of a) the gas-phase and b) liquid-phase setups.

3. Results and discussion

The cyclic voltammetry (CV) profiles reported in Figures 2a and b were recorded under the same experimental conditions as for the photo-electrocatalytic tests, by scanning the potential from -0.25 V to +1.5 V at a rate of 0.05 V s^{-1}, with and without light irradiation. Figure 2a shows the CV recorded in the gas-phase (GP) configuration, while Figure 2b refers to the liquid-phase (LP) configuration. In both setups, light irradiation enhanced the current density values, with the effect being more pronounced in the LP reactor due to the higher conductivity of the liquid electrolyte compared to the vapour phase.

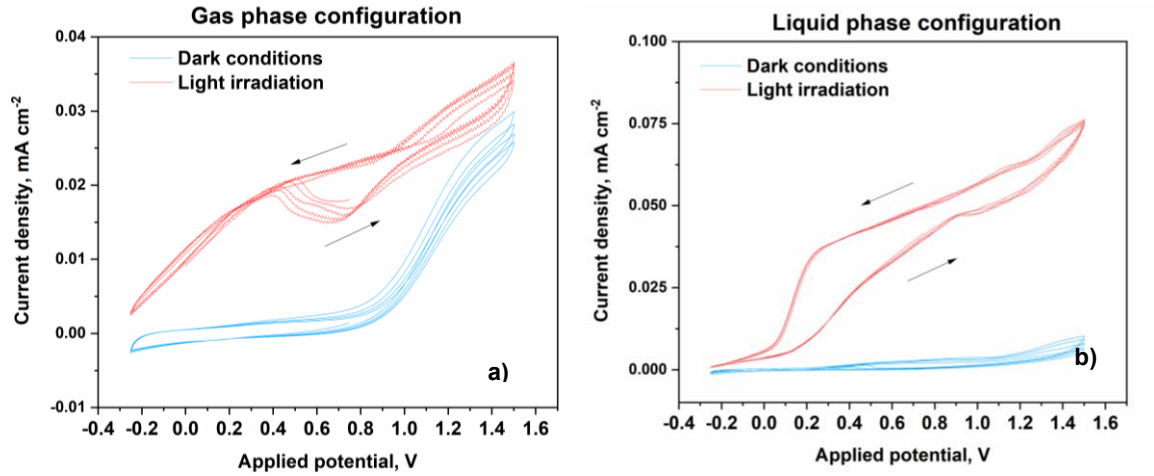

Figure 2: Cyclic voltammetry (CV) profiles performed in a) gas-phase and b) liquid-phase configuration, in dark and under light irradiation conditions. The arrows indicate the direction of the measurements.

Electrochemical impedance spectroscopy (EIS) analysis was performed in both gas- and liquid-phase configurations to evaluate charge transfer phenomena at the electrode surface, which strongly influence the electrochemical behavior (Enache et al., 2006; MacDonald, 1987). The measurements were conducted under light and dark conditions at applied potentials of +0.4 V, +0.8 V, +1.0 V, and +1.4 V, with frequencies scanned from 10000 Hz to 0.1 Hz. Data fitting was performed using Zview® software, using one-constant and two-constant circuit models shown in Figure 3.

In the GP configuration, both dark and EIS data were modelled using the simple one-constant circuit. In the LP configuration, the two-constant circuit model was used (Giusi et al., 2022). While the series resistance (R_s) is related to the cell's electrical connections, the charge transfer resistance (R_{ct}) is associated with the electrochemical reactions, including phenomena occurring at the electrode surface. For the LP process, an additional R_{ct}' was thus determined at high frequency, which is related to charge transfer in the liquid electrolyte.

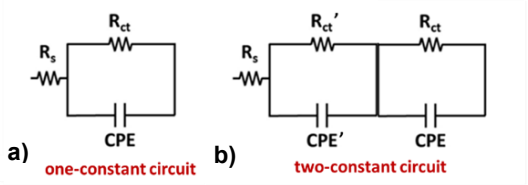

Figure 3: a) one constant circuit and b) two constant circuit models used to fit EIS data.

Figures 4a, b, c and d show the Nyquist plots of EIS data with and without light irradiation, in liquid phase and in gas phase conditions. Table 1 summarizes the R_{ct} values derived from the diameter of the semicircle in the Nyquist plots, obtained via EIS fitting in GP and LP configurations under light irradiation at various applied potentials. For the LP configuration, the low-frequency R_{ct} was considered.
As expected for photoactive materials, R_{ct} values were lower under light irradiation at all applied potentials, in agreement with previous results for TiO_2NTs (De Pasquale et al. 2023). Resistance values were higher in the GP configuration than in the LP, consistent with the higher current density values observed in CV measurements in the LP configuration.

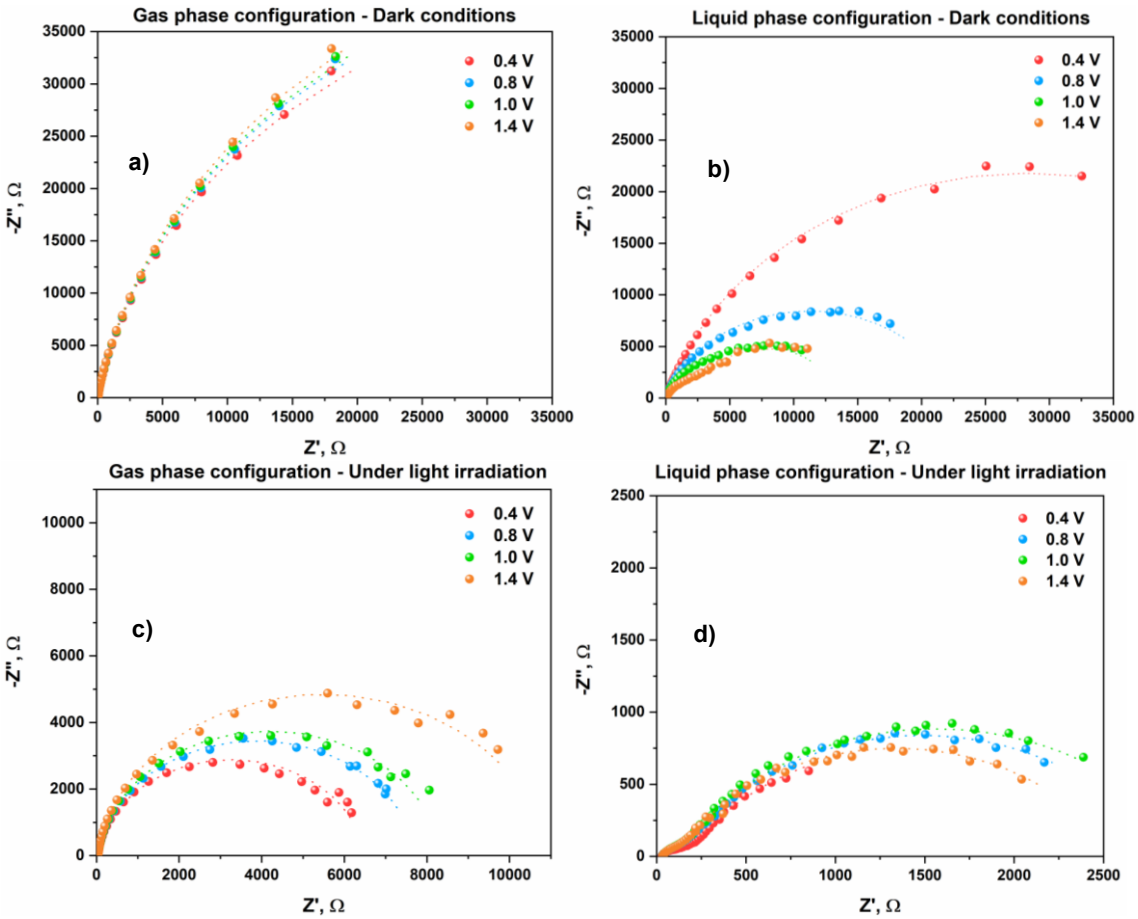

Figure 4: Nyquist plots a) in gas-phase configuration under dark conditions; b) in liquid-phase configuration under dark conditions ; c) in gas-phase configuration under light irradiation; and d) in liquid-phase configuration under light irradiation. Filled symbols represent experimental EIS data; dotted lines represent fitting data by modelling.

Table 1: Charge transfer resistance (R_{ct}) values acquired from EIS fitting under light irradiation in gas and liquid phase at different applied potentials. For liquid phase the low-frequency R_{ct} was considered.

Applied potential (V)	Gas phase R_{ct} (Ω)	Liquid phase R_{ct} (Ω)
0.4	6456	2604
0.8	7692	2684
1.0	8314	2875
1.4	10869	2460

The photo-electrocatalytic tests were performed in the GP and LP configurations for 120 minutes, applying +1 V between the working and counter electrodes, and irradiating the cell with the open spectrum of the lamp. Table 2 summarizes the results in terms of productivities of acetaldehyde, acetic acid, and hydrogen.
No carbon dioxide (CO_2), carbon monoxide (CO) or methane (CH_4) were detected during the tests, indicating that ethanol (or acetaldehyde) complete oxidation (i.e., photo-reforming) was negligible. The reactor configuration had a strong impact on catalytic behaviour, particularly on selectivity. Acetaldehyde was produced in both configurations via ethanol photo-dehydrogenation of ethanol, with productivity of 4.2 μmol h^{-1} in the gas phase and 13.3 μmol h^{-1} in the liquid phase. Notably, no acetic acid was detected in the GP configuration, while a productivity of 0.4 μmol h^{-1} was obtained in the LP configuration due to further oxidation of acetaldehyde to acetic acid.The acetaldehyde formation mechanism on TiO_2-based materials under UV light has been widely studied (Reztsova et al., 1999; Wahab et al., 2014) and involves the following steps i) adsorption of ethanol molecules on the TiO_2 surface, leading to O-H bond dissociation on Ti-O and formation of ethoxy and hydroxyl groups; ii) reaction of hydroxyl groups with holes h^+ to produce OH radicals; iii) reaction of OH radicals with ethoxy species to generate acetaldehyde radicals; iv) the desorption of acetaldehyde radicals after losing one electron.Acetic acid is formed through the further oxidation of acetaldehyde, but it is not generally detected with TiO_2-based catalysts (Giusi et al., 2022)

Table 2: Acetaldehyde, acetic acid and hydrogen productivities during the tests in liquid- and gas-phase configurations.

Cell configuration	Acetaldehyde productivity (μmol h^{-1})	Acetic acid productivity (μmol h^{-1})	Hydrogen productivity (μmol h^{-1})
Liquid-phase	13.3	0.4	6.5
Gas-phase	4.2	0	11.2

4. Conclusions

A TiO_2NT/Ti mesh electrode was used to study the effect of the presence or absence of a liquid electrolyte on catalytic performance in the process of ethanol photo-dehydrogenation. For this purpose, a versatile photo-electrochemical (PEC) cell capable of operating in either liquid- or gas-phase configurations was designed.
The results demonstrated that the presence of a liquid electrolyte significantly influenced both the type and quantity of products formed at the anode during ethanol photo-conversion. Interestingly, acetic acid formation was observed exclusively in the liquid-phase configuration, whereas it was absent in the gas phase that provided a higher carbon selectivity to acetaldehyde.
In conclusion, varying the reactor configuration led to distinct reaction pathways in ethanol photo-dehydrogenation, resulting in different product selectivity. This study highlights that photo-catalytic performance is determined not only by the catalyst's intrinsic properties but also by reactor design and configuration, emphasizing the critical role of system engineering in catalytic processes.

Acknowledgments

This work was funded by the European Union through the H2020 Projects “SUPERVAL” (ID: 101115456) and SCOPE (ID: 810182), and by the Italian Ministry for Universities and Research (MUR) through the FISA Project “SCOOP” (FISA-2022-00277) and NEST Spoke 9 Project “eCO_2”, which are gratefully acknowledged.

References

Ampelli C., Tavella F., Giusi D., Ronsisvalle A.M., Perathoner S., Centi G., 2023, Electrode and cell design for CO2 reduction: A viewpoint, Catalysis Today, 421, 114217.

De Pasquale L., Tavella F., Longo V., Favaro M., Perathoner S., Centi G., Ampelli C., Genovese C., 2023, The Role of Substrate Surface Geometry in the Photo-Electrochemical Behaviour of Supported TiO2 Nanotube Arrays: A Study Using Electrochemical Impedance Spectroscopy (EIS), Molecules, 28, 3378.

Enache D. I., Edwards J.K., Landon P., Solsona-Espriu B., Carley A.F., Herzing A.A., Watanabe M., Kiely C.J., Knight D.W., Hutchings G.J., 2006, Solvent-Free Oxidation of Primary Alcohols to Aldehydes Using Au-Pd/TiO2 Catalysts, Science, 311, 362–365.

Giusi D., Miceli M., Genovese C., Centi G., Perathoner S., Ampelli C., 2022, In situ electrochemical characterization of CuxO-based gas-diffusion electrodes (GDEs) for CO2 electrocatalytic reduction in presence and absence of liquid electrolyte and relationship with C2+ products formation, Applied Catalysis B, 318, 121845.

Giusi D., Tavella F., Miceli M., Ronsisvalle A.M., Costantino V., Ampelli C., 2023, Copper Oxide onto Gas Diffusion Electrodes to Enhance Selectivity towards >C1 Chemicals in Gas-phase CO2 Electrocatalytic Reduction, Chemical Engineering Transactions, 100, 643-648.

Hu A., Tao F., Jie Y., Yuefei H., Shungui Z., Bing L., Guangqian W., 2024, Photoelectrochemical methane production achieved energy recovery from wastewater with low organic concentration, Chemical Engineering Journal, 500, 157113.

Hu Q., Fan L., Gao D., 2017, Pilot-scale investigation on the treatment of cellulosic ethanol biorefinery wastewater, Chemical Engineering Journal, 309, 409-416.

Lima Perini J.A., Tavella F., Ferreira Neto E.P., Boldrin Zanoni M.V., Lima Ribeiro S. J., Giusi D., Centi G., Perathoner S., Ampelli C., 2021, Role of nanostructure in the behaviour of BiVO4-TiO2 nanotube photoanodes for solar water splitting in relation to operational conditions, Solar Energy & Solar Cells, 223, 110980.

MacDonald J.R., 1987, Impedance Spectroscopy, Wiley-Interscience, New York, USA.

Nabgan W., Alqaraghuli H., Owgi A.H.K., Ikram M., Vo D.V.N., Jalil A.A., Djellabi R., Nordin A.N., Medina F., 2024, A review on the design of nanostructure-based materials for photoelectrochemical hydrogen generation from wastewater: Bibliometric analysis, mechanisms, prospective, and challenges, International Journal of Hydrogen Energy 52, 622-663.

Reztsova T., Chang C.-H., Koresh J., Idriss H., 1999, Dark- and Photoreactions of Ethanol and Acetaldehyde over TiO2/Carbon Molecular Sieve Fibers, J Catal, 185, 223–235.

Saboo T., Tavella F., Ampelli C., Perathoner S., Genovese C., Marepally B.C., Veyre L., Quadrelli E.A., Centi G., 2018, Water splitting on 3D-type meso/macro porous structured photoanodes based on Ti mesh Solar Energy Materials & Solar Cells, 178, 98–105.

Verma G., Rai P.K., Korvink J. G., Islam M., Gupta A., 2022, Integrated electrochemical and photocatalytic degradation using ZnO caterpillars photocatalyst: Two-step approach for textile industry based wastewater recovery, Materials Science & Engineering B, 116078.

Wahab A.K., Bashir S., Al-Salik Y., Idriss H., 2014, Ethanol photoreactions over Au–Pd/TiO2, Appl Petrochem Res, 4, 55–62.

Wei Z., Qin Y., Li X., Gao P., 2024., Resource recovery of high value-added products from wastewater: Current status and prospects, Bioresource Technology, 398, 130521.

Yadav A., Rene E. R., Sharma M., Jatain I., Mandal M. K., Dubey K. K., 2022, Valorization of wastewater to recover value-added products: A comprehensive insight and perspective on different technologies, Environmental Research, 214, 2.